Powder Metallurgy and Metal Ceramics, Vol. 36, Nos. 5,6, 1997

PHASE EQUILIBRIA IN THE Cr–Ni–C SYSTEM AND THEIR USE FOR DEVELOPING PHYSICOCHEMICAL PRINCIPLES FOR DESIGN OF HARD ALLOYS BASED ON CHROMIUM CARBIDE

A. A. Bondar, V. A. Maslyuk, T. Ya. Velikanova, and A. V. Grytsiv

UDC 669.017.3:669.26'24'784:666.018.95

The Cr–Ni–C phase diagram at the melting point was plotted by a combination of procedures (metallography, x-ray, microprobe, differential thermal analysis, Pirani–Alterthum method, etc.). A general feature of this system is the existence of equilibria between the nickel-based phase and all the other phases. The temperature of the quasibinary (Ni) + (Cr_7C_3) eutectic was determined to be 1324 ± 6°C. Based on both the phase diagram of the Cr–Ni–C system and the bending strength and Rockwell hardness of the alloys, the optimal composition of the initial carbide ingredient for production of hard alloys based on Cr_3C_2 with nickel–phosphorus binder was estimated as 13.0-13.3 at.%, substoichiometric with respect to Cr_3C_2.

Hard alloys based on chromium carbide with nickel (KKhN) and nickel–phosphorus (KKhNF) binders, owing to their high hardness, wear and corrosion resistance, are some of the few materials that can be used under conditions of simultaneous action of several factors: friction, abrasive wear, corrosive medium, and elevated temperature [84Mac]. The hard component of these materials, which is either the phase based on chromium carbide (Cr_3C_2)* or a mixture of (Cr_3C_2) and (Cr_7C_3), are 70-95 mass % of the total; the rest is the carburizing binder. Alloys containing 15-20 mass % metal binder have had the broadest practical application, owing to the optimal values of the hardness and wear resistance and rather high strength characteristics. In order to increase the strength, chromium carbide hard alloys are alloyed with small additions of phosphorus, generally 0.1-0.15 mass %. Phosphorus is a surface-active element relative to nickel and an interphase-active element relative to chromium. So it activates solid-phase diffusion of nickel in Cr_3C_2, improves the wettability of chromium carbide by the melt, and enhances the strength of the adhesive bond between the components [78Kli]. This results in a 40-60% increase in the bending breaking stress and the impact toughness of KKhNF alloys, and thus extension of their range of application. Thus, this wear-resistant material is effectively used for manufacturing working parts of tool attachments used in pressing articles made of ferrite powder, in the production of dies for drawing steel channel sections and copper wire, for manufacturing valve seats for oil well pumps, the working elements of grinders, a diamond rock-crushing tool, and other articles. The useful service life of such parts increases by a factor of 7-14.5 compared with articles made from carbon and tool steels. When using 1 ton of chromium carbide alloys, we can save up to 14.5 tons of steel rolled stock and up to 1.2 tons of very scarce tungsten used to manufacture tungsten–cobalt hard alloys [77Kli]. An advantage of hard alloys based on chromium carbide, in addition to the advantages indicated above, is the availability and relatively low cost of the starting components. The shortage of tungsten and cobalt-containing raw material, which is becoming more acute every year, and also the lack of deposits of these metals in Ukraine which can be developed have been a considerable stimulus to the search for new and improvement of existing tungsten-free hard alloys, including chromium carbide alloys.

The composition of KKhN and KKhNF alloys and technology for obtaining them have been well worked out over the course of more than 35 years of production. However, despite undoubted successes achieved in optimization of the structure and physicomechanical properties of alloys, extension of the volume and areas of application of the materials has been held

*Parentheses mean a solid solution based on the indicated phase, in this case $(Cr,Ni)_3C_2$.

Institute of Problems in Materials Science, National Academy of Sciences of Ukraine, Kiev. Translated from Poroshkovaya Metallurgiya, No. 5/6(395), pp. 13-24, May-June, 1997.

 1068-1302/97/3656-0242$18.00

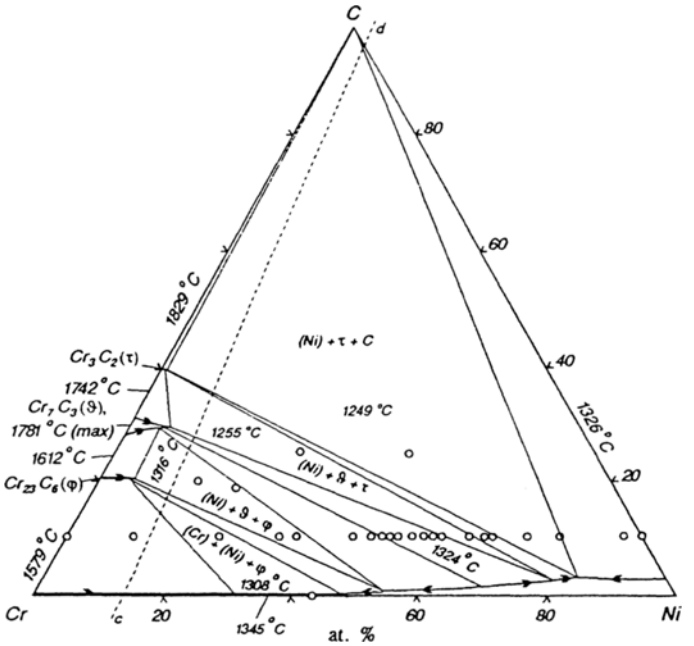

Fig. 1. Projection of the solidus surface of the Cr−Ni−C system.

back due to their basic disadvantage: the instability of the strength properties. In order to eliminate this disadvantage, we need to develop ideas about regular trends in the physicomechanical features of the interaction of chromium carbide with metals of the iron family, especially with nickel and its alloys. The morphology and physicomechanical properties of chromium carbide−nickel powder alloys are determined by the content and composition of the carburizing binder, the phase composition of the carbide component, and the grain size of the phases. Since chromium carbide−nickel alloys are obtained over the course of liquid-phase sintering, in which they practically completely achieve the equilibrium state, first and foremost we need to know the phase diagrams of the Cr−Ni−C and Cr−Ni−C−P systems in the melting−crystallization region. The phase diagram of the Cr−Ni−C−P system has not been studied. Considering the low phosphorus content in commercial alloys, we have a basis for assuming that the phase equilibria in a system with phosphorus in the region of compositions used for preparation of KKhNF alloys are not very different from the phase equilibria in the Cr−Ni−C system. Since V. V. Grigor'eva and V. N. Klimenko [61Gri] have shown that along with other factors, the characteristics of the carbide component considerably affect the bending breaking stress and the scaling resistance of chromium carbide−nickel alloys, an objective need arises to refine the phase equilibria in the Cr−Ni−C with the goal of using such equilibria to develop physicochemical principles for designing hard alloys based on chromium carbide.

Phase equilibria have been repeatedly studied both in the ternary Cr−Ni−C system (data are presented in the handbook [95Ter] from [40Mur, 55Kos, 71Tel, 82Tum] with no commentaries) and in binary limiting systems [Mas2]. We have taken the phase diagrams for Ni−C and Ni−Cr binary systems from [Mas2], where the phase diagram for Ni−C was published from the results of the review [89Sin]; the Ni−Cr diagram was taken from [86Nas, 91Nas]. For the Cr−C system, in contrast to [Mas2], where the phase diagram based on data in [69Rud] was taken from the review [90Ven], we used the higher temperatures for the nonvariant equilibria we obtained earlier in [87Ere].

For the Cr−Ni−C system, isothermal sections have been published for 800°C [55Kos], 1000°C [82Tum], 1100°C [71Tel, 82Tum], and 1200°C [82Tum]; also the projection of the liquidus surface [40Mur, 55Kos] and polythermal cross sections along carbon isoconcentrates 0.5, 1.8, 4, and 6.5 mass % have been published [40Mur]. However, despite such a large number of investigations, the phase diagram for the Cr−Ni−C system cannot be considered as reliably plotted over the entire range of concentrations and temperatures. Thus the authors of [74Lob, 75Tum, 81Ale, 82Tum] have carried out thorough investigations of alloys near the region of homogeneity of the solid solution based on nickel for temperatures 1000-1200°C, but for the rest of the concentration range the isothermal sections are tentative. Data in [40Mur] and 55Kos] on the phase equilibria in the melting−crystallization region of the alloys are quite different. Analysis of the reasons for the discrepancy is difficult because [40Mur] is not available to us. The use of insufficiently pure materials in [55Kos] (chromium with 5 mass

TABLE 1. Phase Composition at Subsolidus Temperatures and Phase Transition Temperatures for Alloys in the Cr–Ni–C System

Alloy composition, at. %		Phase composition*	Solidus temperature, °C					
			by Pirani–Alterthum					by DTA
Cr	C		t_{pyr}**	t_{true}	$\pm D_{stat}$	$\pm D_{tot}$	n	
80	10	(Cr) + φ	1434	1442	6	7	5	1420
66	10	(Cr)+φ+(Ni)	1301	1308	1	4	5	1328
65	20	φ + ϑ + (Ni)	1304	1310	1	4	5	1336
59	18	Same	1304	1310	5	6	4	1332
56	10	Same	1315	1325	6	7	5	1329
54	10	Same	1310	1316	1	4	5	1338
45	10	ϑ + (Ni)	1309	1316	3	6	4	1334
42	10	Same	—	—	—	—	—	1339
40	10	Same	1312	1325	5	6	6	1340
39	10	Same	1303	1316	2	4	4	1339
38	10	Same	1306	1318	3	4	3	1340
36	10	Same	1305	1312	2	4	5	1328
34	10	Same	1300	1307	3	5	5	1316
32,5	10	Same	1284	1290	2	4	5	1291
31,5	10	Same	1278	1285	3	5	5	—
46	25	ϑ + τ + (Ni)	1242	1252	3	5	5	1267
27	10	Same	1254	1261	4	6	4	1267
24	10	τ + (Ni)	1246	1257	3	5	4	—
23	10	Same	1249	1256	2	5	4	1253
29	25	τ + (Ni) + C	1235	1246	2	4	4	1236
18	10	Same	1229	1240	12	13	4	1242
13	10	Same	1265	1269	24	24	3	1232
3	10	(Ni) + C	1313	1319	6	7	2	1311
0	90	Same	1317	1329	2	4	3	1340
56	0	(Cr) + (Ni)	1333	1345	5	6	5	1318

*The phase symbols are given in Fig. 1. **t_{pyr} and t_{true} are the pyrometric and true temperature of onset of melting (solidus), Δ_{stat} and Δ_{tot} are the statistical and total measurement errors, n is the number of measurements.

% Fe) and an insufficiently correct method for determining the temperatures of the nonvariant equilibria along the cooling curve (which generally makes the results too low) raises doubts about the reliability of the data obtained. At the same time, analysis of the phase diagram performed earlier [93Bon] for a number of KKhN alloys shows that even small changes in their composition lead to substantial changes in the phase composition and properties. So we plotted the phase diagram in the melting–crystallization region for the alloys again from the results obtained in our experimental investigation.

INVESTIGATION OF PHASE EQUILIBRIA

Ternary alloys of 23 compositions (Fig. 1, Table 1) were smelted in a laboratory arc furnace with unconsumed tungsten electrode on a copper water-cooled hearth in argon medium (pressure about 80 kPa), gettered by molten titanium for 3 min. The mix of mass 10-15 g was presintered with a weak arc and then remelted twice with turning. Then the ingots were ground and were melted a second time in this way. The cooling rate was about 100 deg/sec. The mass losses in melting were no greater than 0.5%, so the composition of the alloys were assumed to be as in the mix. The starting materials were grade ÉRKh grade chromium (99.9 mass % Cr), PNK-5 nickel (no less than 99.5% Ni), and graphite, ash content 0.05 at.%. We used $Ni_{90}C_{10}$, $Cr_{90}C_{10}$, and $Cr_{50.3}C_{40.7}$ master alloy, carefully monitoring the compositions by chemical analysis.

Cast alloys annealed at a subsolidus temperature were investigated by the metallography (optical and scanning electron microscopy) and x-ray phase analysis. The x-ray patterns for ground specimens were taken in RKD-57,3 cameras using Cu$K\alpha$- and Cr$K\alpha$-radiation. The lattice periods were calculated using an updated Cohen–Hess method [51Hes]. The values of the periods are given with confidence interval $\alpha = 0.95$ for the reliability (Table 2). The composition of the phases in equilibrium and the eutectics were determined by local x-ray spectral analysis on a Jeol Superprobe-733. Since the error in measuring the carbon content by this method is substantially higher than the error in measuring the metal content, we determined only the ratio of the metal contents.

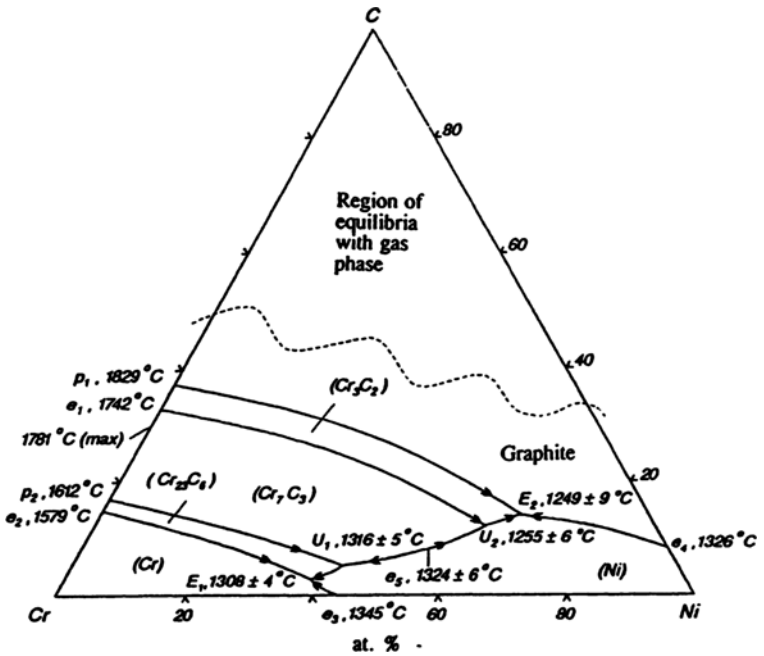

Fig. 2. Projection of the liquidus surface of the Cr−Ni−C system.

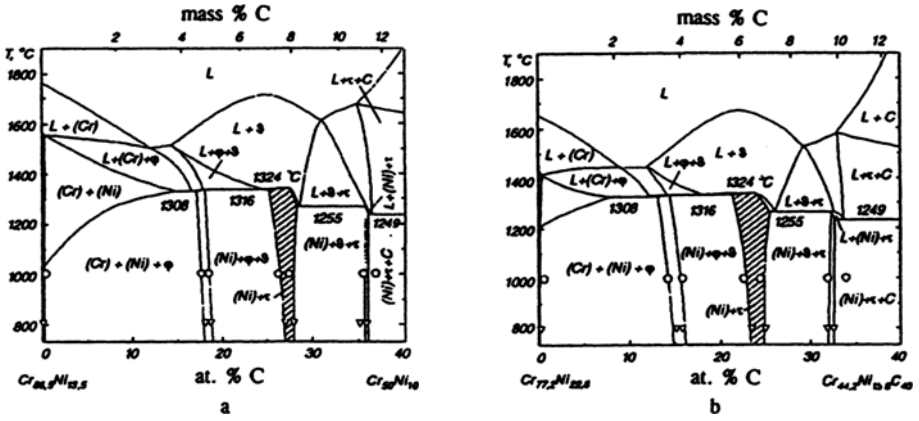

Fig. 3. Polythermal sections of the phase diagram for the Cr−Ni−C system along nickel isoconcentrates. *a*) 15 mass %, denoted as *cd* in Fig. 1; *b*) 25 mass %; *1*) position of phase boundaries according to data in [71Tel]; *2*) same, according to [55Kos]; the (Cr_3C_2) + (Ni) region is hatched.

The temperatures of the phase transitions all the way to the liquidus temperatures were determined by differential thermal analysis on an apparatus with a cable thermocouple designed by Yu. A. Kocherzhinskii [71Koch]. The DTA was done with heating and cooling rate of about 60 deg/min in high-purity helium medium, using alundum crucibles. The tungsten/BP-20 thermocouple was calibrated using an MPTSh-90 reference (Al, Au, Pd, Pt, Rd), and also an auxiliary reference (Fe, Si, and others). In averaging the results of a series of measurements, we calculated only the statistical error of the determination $D_{stat}(\alpha = 0.95)$, since in this method taking instrumental error into account is quite problematic (Table 1).

Furthermore, the temperature of onset of melting (the solidus temperature) was measured by the Pirani−Alterthum method [23Pir] (Table 1). The sample was heated in high-purity helium. It took from 10 to 50 min to make the measurements. Immediately after this, the specimen was annealed for 30 min at a temperature 20-40°C below the solidus. The cooling rate was about 200-300 deg/sec. The pyrometric temperature for onset of melting t_{pyr} (Table 1) was measured by an ÉOP-68 pyrometer (instrumental error ±2.8°C at 900-1400°C). The number of measurements n that were made on a single specimen was usually 3-5. In Table 1 we give the results of statistical treatment Δ_{stat} for these data. The pyrometric temperature was too low compared with the true t_{true} because of two factors: absorption of radiation by the viewing window and the fact that

TABLE 2. Lattice Periods of Phases in Nonvariant Equilibria on the Solidus Surface in the Cr–Ni–C System

Phase region	Phase	Lattice periods, pm		
		a	*b*	*c*
(Cr) + (Ni) + φ	(Cr)	286,5 ± 0,2	—	—
	(Ni)	359,8 ± 0,1	—	—
	φ	1068,7 ± 0,7	—	—
φ + ϑ + (Ni)	φ	1064,3 ± 0,3	—	—
	(Ni)	357,8 ± 0,3	—	—
	ϑ	1402,6 ± 0,3	—	452,1 ± 0,3
ϑ + (Ni)	ϑ	1402,4 ± 0,5	—	451,9 ± 0,5
	(Ni)	356,1 ± 0,1	—	—
ϑ + τ + (Ni)	ϑ	1401 ± 2,0	—	448 ± 2,0
	τ	554,4 ± 0,5	283,1 ± 0,6	1146 ± 2
	(Ni)	355,0 ± 0,3	—	—
τ + (Ni) + C	τ	553,7 ± 0,5	283,1 ± 0,5	1148 ± 2,0
	(Ni)	354,64 ± 0,05	—	—

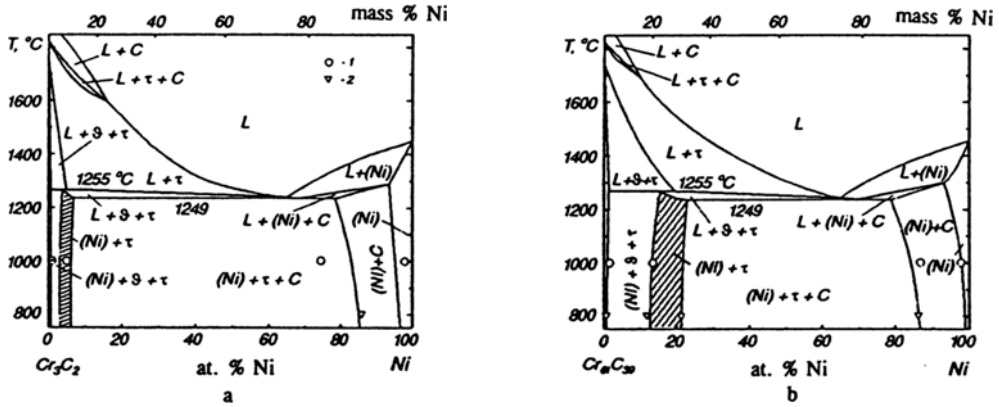

Fig. 4. Polythermal sections of phase diagram of Cr–Ni–C system along the paths Ni–Cr_3C_2 (*a*) and Ni–$Cr_{61}C_{39}$ (*b*). *1*) position of phase boundaries according to data in [71Tel]; *2*) same according to [55Kos]; the (Cr_3C_2) + (Ni) region is hatched.

blackbody conditions are not satisfied in the model used (a blind hole in the specimen with ratio of depth to diameter of approximately 4:1). Corrections were introduced using the formula

$$\frac{1}{T_0} = \frac{1}{T_1} + A,$$

where $T_0 = t_{true} + 273.15$; $T_1 = t_{pyr} + 273.15$. For the viewing window, $A = -(3.7 \pm 0.5) \cdot 10^{-6}$ °K^{-1}. The correction for nonideality of the model is:

$$A = (\lambda / C_2) \lg \varepsilon_{0.65},$$

where $\lambda = 0.65$ μm; $C_2 = 1.4388 \cdot 10^4$ μm·°K; $\varepsilon_{0.65}$ is the emissivity of the blind hole. The latter value, depending on the ratio of the depth of the hole to the diameter and on the emissivity of the material, is taken from [64Lis]. In this case, the emissivity of alloys of the Cr–Ni–C system is estimated from the additivity rule from the properties of the pure components. The total error in measurement of the temperature Δ_{tot} was determined taking into account the statistical error, the instrumental errors of the pyrometer and ammeter, and also the errors in introduction of the corrections ($\alpha = 0.95$).

The basic data on the phase composition and temperatures of the phase transition are given in Table 1; the compositions of the phases in equilibrium are given in Table 3. The results obtained served as the basis for plotting the phase diagram as

TABLE 3. Nonvariant Equilibria in the Cr–Ni–C System

Nonvariant equilibrium	Phase	Phase composition, at. %		
		Cr	Ni	C
E_1, 1249±9 °C	L	20,0	66,0	14,0
$L \rightleftharpoons$ (Ni) + τ + C	(Ni)	13,6	83,4	3,0
	τ	59,3	0,7	40,0
	C	0	0	100,0
U_1,1255±6 °C	L	26,0	62,0	12,0
L + ϑ $\rightleftharpoons$ (Ni) + τ	ϑ	64,0	6,0	30,0
	(Ni)	17,6	79,9	2,5
	τ	59,4	0,6	40,0
E_2,1308±4 °C	L	59,0	38,0	3,0
$L \rightleftharpoons$ φ + (Cr) + (Ni)	φ	75,3	4,0	20,7
	(Cr)	68,0	31,8	0,2
	(Ni)	52,0	47,5	0,5
U_2,1316±5 °C	L	53,0	42,0	5,0
L + ϑ $\rightleftharpoons$ (Ni) + φ	ϑ	65,8	4,5	29,7
	(Ni)	45,0	54,0	1,0
	φ	74,3	5,0	20,7
e_n,1324±6 °C	L	37,7	54,3	8,0
$L \rightleftharpoons$ (Ni) + ϑ	(Ni)	29,5	69,0	1,5
	ϑ	65,0	5,0	30,0

projections of the solidus and liquidus surfaces (Figs. 1 and 2) and also a number of polythermal sections (Figs. 3 and 4). The composition and periods of the phases in nonvariant equilibria are given in Tables 2 and 3.

Comparison of the statistically treated data from the DTA and Pirani–Alterthum methods on the temperatures of the nonvariant equilibria reveals some differences between them, with overall good agreement (Table 4). Since the DTA method involves a number of uncertain errors that are difficult to take into account (for example, the change in the melting point of the references during use in connection with contamination by carbon and(or) chromium), the temperatures of the nonvariant equilibria were assumed to be those obtained by the Pirani–Alterthum method (Tables 3 and 4). Our results are quite consistent with [40Mur] (Table 4).

Based on the results obtained in this paper and literature data, we can consider it to be conclusively established that in the ternary Cr–Ni–C system there are no phases with a structure different from binary (ternary compounds). The greatest extent of the regions of homogeneity is observed for solid solutions based on metallic components. We estimated the solubility of carbon based on the literature data. The maximum solubility of carbon in (Ni) obtained by extrapolation of data in [82Tum] to the solidus temperature (about 3 at.%) fits the composition found in equilibrium with (Cr_3C_2) and graphite. The solubility of carbon in (Ni) decreases with an increase in the chromium content and is approximately 1 at.% for the composition in equilibrium with (Cr) and ($Cr_{23}C_6$). No one has specially studied the solubility of carbon in the phase based on chromium in the ternary Cr–Ni–C system. At the solidus temperature, it probably should not exceed the maximum solubility in the binary Cr–C system, i.e., 0.4 at. %, according to the data in [77Pou, 85Pou]. According to our data, obtained by the local x-ray spectral analysis method (Table 3), the maximum solubility of nickel in $Cr_{23}C_6$ is 5 at.%; in Cr_7C_3, 6 at.%; and in Cr_3C_2, 0.7 at.%.

The liquidus surface (Fig. 2) consists of regions of primary crystallization of six phases. The primary crystallization field of graphite is bounded from above (with respect to carbon) by a region of phase equilibria with participation of a gas phase, which was not studied in this work. The saddle point on the line for cocrystallization of the phases (Cr_7C_3) and (Ni) on the liquidus surface corresponds to the plait point of the temperature maxima on the ruled surface of the (Cr_7C_3) + (Ni) solidus (Fig. 1). This maximum is rather faint. So in order to observe it, we carried out special experiments on a DTA apparatus. Two alloys were simultaneously placed into the measurement block: one as the specimen, the second as the reference. In the second run, we switched their positions. The more refractory alloy in both cases was the second one to begin to melt. The melting point of the alloy $Cr_{40}Ni_{50}C_{10}$ determined this way, 1340°C (which agrees with the data from the Pirani–Alterthum method, Table 1), corresponds to a three-phase nonvariant eutectic equilibrium: $L_e \rightleftarrows (Cr_7C_3) + (Ni)$.

We should note that the section along the tie line on which this quasibinary eutectic is found, $Cr_{67.8}C_{32.2}$–$Cr_{27.6}Ni_{72.4}$, is partially quasibinary. Singular triangulation of the phase diagram cannot be done along this, since it does not pass through the dystectic points of the phases (Cr_7C_3) and (Ni), but rather in the Cr–C binary system goes to a two-phase region Cr_7C_3+Cr_3C_2.

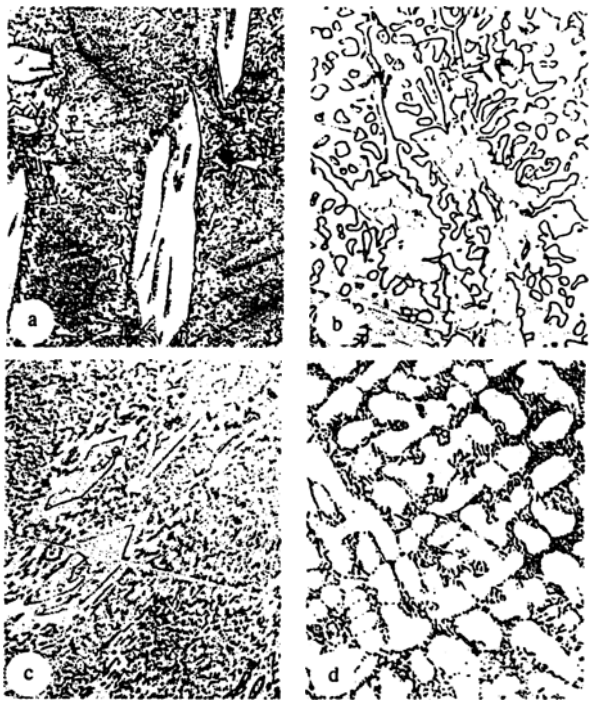

Fig. 5. Microstructure of alloys of the system Cr–Ni–C, ×300. *a*) $Cr_{56}Ni_{34}C_{10}$, cast, primary (Cr_7C_3), eutectics (Ni) + (Cr_7C_3), (Ni) + $(Cr_{23}C_6)$, and (Ni) + $(Cr_{23}C_6)$ + (Cr); (*b*) same, annealed at 1305°C, 30 min, (Cr_7C_3) + (Ni) + $(Cr_{23}C_6)$; *c*) $Cr_{40}Ni_{50}C_{10}$, cast, primary (Cr_7C_3) and eutectic (Ni) + (Cr_7C_3); *d*) $Cr_{67}Ni_{23}C_{10}$, cast, primary (Ni) and eutectics (Ni) + (Cr_3C_2) and (Ni) + (Cr_3C_2) + C.

The results of analysis of the values obtained for the solidus temperatures and the conclusions concerning eutectic cocrystallization of alloys of the two-phase region (Ni) + (Cr_7C_3) and three-phase (Ni) + (Cr_7C_3) + (Cr_3C_2) and (Ni) + (Cr_3C_2) + C (Figs. 1 and 2) are consistent with the metallography data. A number of typical examples are presented in Fig. 5. The cast alloy $Cr_{56}Ni_{34}C_{10}$ (Fig. 5*a*) contains grains of primary crystallized phase (Cr_7C_3) in a eutectic matrix. According to local x-ray spectral analysis data, the most highly dispersed eutectic colonies are (Ni) + (Cr) + $(Cr_{23}C_6)$. The (Cr_7C_3) grains are surrounded by less differentiated eutectics (Ni) + (Cr_7C_3) and (Ni) + $(Cr_{23}C_6)$. The presence in this alloy of the eutectics (Ni) + (Cr) + $(Cr_{23}C_6)$ and (Ni) + $(Cr_{23}C_6)$ is explained by nonequilibrium crystallization of the alloy. After annealing for 30 min at a subsolidus temperature (1305°C), the eutectic matrix is considerably coarsened, as shown in Fig. 5*b*, and the specimen becomes three-phase (Ni) + $(Cr_{23}C_6)$ + (Cr_7C_3). According to the local x-ray spectral data (Table 3), the carbide $Cr_{23}C_6$ dissolves 5 at.% Ni, the solid solution (Ni) dissolves 45 at.% Cr. In Fig. 5*c*, we present the structure of the cast two-phase alloy $Cr_{40}Ni_{50}C_{10}$, the composition point of which lies on the line of the degenerate tie-line triangle of the quasibinary eutectic (Ni) + (Cr_7C_3). The primary crystallized grains of (Cr_7C_3) with characteristic ring-shaped structure lie in a homogeneous eutectic matrix. In Fig. 5*d*, we present the microstructure of the cast alloy $Cr_{67}Ni_{23}C_{10}$. In the state annealed at a subsolidus temperature, it is two-phase (Ni) + (Cr_3C_2): it contains primary grains of (Ni) phase in a eutectic matrix.

Of special interest are the polythermal sections, which pass through the composition regions of the commercial KKhN (KKhNF) alloys. So here we present the path sections Ni–$Cr_{61}C_{39}$ and Ni–Cr_3C_2 (Fig. 3*a*, *b*) and the section along the 15 mass % and 25 mass % nickel isoconcentrates (Fig. 4*a*,*b*). From the figures we see that alloys of the phase composition (Ni) + (Cr_3C_2) can be obtained only in a narrow interval of alloy composition. Relatively small variations (especially with respect to carbon content) substantially change the phase composition of the alloys and (as will be shown below) their properties.

TABLE 4. Comparison of Temperatures (°C) of Nonvariant Equilibria in the System Cr–Ni–C Using Data From Different Investigations

Nonvariant equilibrium	Data in this work		Literature data*	
	$t_{true} \pm D_{tot}$	$t_{DTA} \pm D_{stat}$	[40Mur]	[55Kos]
$L \rightleftharpoons$ (Ni) + τ + C	1249±9	1235±6	1240	1045
$L + \vartheta \rightleftharpoons$ (Ni) + τ	1255±6	1267±6	1260	~1220
$L \rightleftharpoons \varphi$ + (Cr) + (Ni)	1308±4	1328	1305	1270
$L + \vartheta \rightleftharpoons$ (Ni) + φ	1316±5	1334±6	1315	~1280
$L \rightleftharpoons$ (Ni) + ϑ	1324±6	1340	—	1305

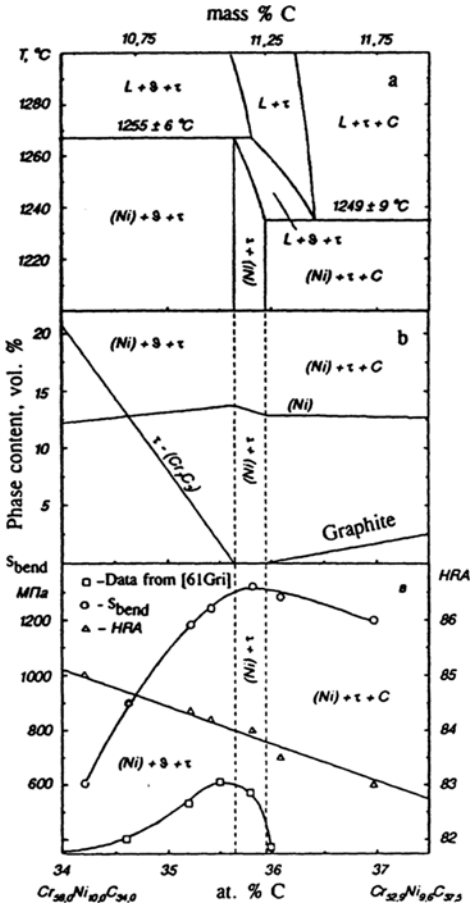

Fig. 6. Fragment of the polythermal section of the phase diagram of the Cr–Ni–C system along the 15 mass % nickel isoconcentrate (*a*), the volume content of the phases in the alloys (*b*), the Rockwell hardness and the bending breaking stress (*c*) for alloys KKhNF-15 and KKhN-15 (our data and [61Gri]).

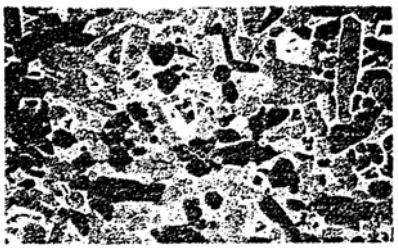

Fig. 7. Microstructure of alloy KKhNF-15 with carbon content in the original carbide component of 13.2 mass %. ×1253.

INVESTIGATION OF THE PHYSICOMECHANICAL PROPERTIES

Hard alloys KKhNF-15 were obtained from chromium carbide produced by the Special Office of Design and Technology of the Institute of Problems in Materials Science, National Academy of Sciences of Ukraine. The total carbon content in the material had various values: 12.4, 12.6, 12.9, 13.0, 13.2, 13.34, and 13.8 mass %. Oxygen impurities were about 0.2 mass %, free carbon (except for carbon-enriched compositions) was about 0.01 mass %. The binder was nickel–phosphorus alloy containing 0.7 mass % P. Phosphorus was introduced in the form of an ammonium biphosphate solution in water. Electrolytic nickel powder moistened with this solution after drying was annealed in hydrogen at 750°C for 2 h. Then the mixture consisting of 85 mass % carbide and 15 mass % binder was ground and mixed for 70 h in a ball mill lined with hard alloy, in ethanol medium. The grinding bodies were balls made of VK-8 hard alloy in 5:1 ratio with the powder. Pressing was done with a load of 150 MPa in a closed mold, using a 3% solution of rubber in gasoline as the plasticizer.

The specimens were sintered in two steps. In the first step, they were heated in a medium of dry hydrogen at 900°C for 1 h and then under a 10^{-2} Pa vacuum at a temperature of 1270°C for 45 min. Preliminary experiments established [78Kli] that such treatments provide maximum shrinkage and density of the alloys. As we see from the phase diagrams (Fig. 1), sintering is accomplished at a temperature only slightly greater than the solidus temperature in the region of nonvariant tie-line triangles (Cr_3C_2) + $(C_{Cr7}C_3)$ + (Ni), 1255 ± 6°C, and (C_3C_2) + (Ni) + C, 1249 ± 9°C, according to our data.

The microstructure, the bending breaking stress, and the Rockwell hardness of the alloys were selected by the optimization parameters. The bending breaking stress was determined according to the standard procedure by fracturing a 5 × 5 × 35 mm specimen freely resting on two supports (the distance between them was 30 mm), under short-term static loading conditions. The Rockwell hardness was measured on at least 10 specimens from a single lot by forcing a diamond conical tip into the specimen at room temperature on a TK-2M tester with a load of 588 ± 1 N (scale A).

In Fig. 6, the measurement results are compared with a fragment of the polythermal section along the 15 mass % nickel isoconcentrate, which is shown in full in Fig. 3*a*, and also with the volume content of the phases in the alloys of the two-phase region (Cr_3C_2) + (Ni) and the conjugate three-phase regions. The molar phase content is calculated starting from the compositions we obtained for the solid solutions (Cr_3C_2) and (Ni), which are in equilibrium with each other and with (CrC_3) or graphite at subsolidus temperatures (Table 3, Fig. 1). Knowing the lattice periods for the phases (Table 2), the molar phase content was converted to volume content (Fig. 6*b*). Note the fact that the volume content of nickel in the alloys of this section varies little within the investigated composition interval, since according to the phase diagram the ratio of the contents of the carbide component and the nickel change very little along this section. In this case, the chemical composition also varies within narrow limits: $Cr_{13.6}Ni_{83.4}C_3$–$Cr_{17.6}Ni_{79.9}C_{2.5}$. At the same time, the ratio of the fraction of carbides substantially depends on the amount of carbon in the alloys (Fig. 6*b*): As the carbon content increases, the (Cr_7C_3) content decreases down to zero at the boundary of the regions (Cr_7C_3) + (Cr_3C_2) + (Ni)/(Cr_3C_2) + (Ni).

As we see from Fig. 6, according to the data in [61Gri] the maximum bending strength is displayed by the KKhN alloy lying in the three-phase region (Cr_7C_3) + (Cr_3C_2) + (Ni) practically at the boundary with the two-phase region (Cr_3C_2) + (Ni). According to our data from this work, the maximum level of the strength properties is obtained for the KKhNP-15 alloy, in which along with the basic phases (Cr_3C_2) + (Ni) we observe the carbide (Cr_7C_3). Evidence for this comes from scanning electron microscopy data obtained on a T-20 microscope and a Superprobe 733 x-ray microanalyzer (Fig. 7). The curve showing the concentration dependence of the bending strength of the KKhNP-15 alloys, plotted in Fig. 6 for compari-

son with the data in [61Gri], has a pronounced maximum: 1320 MPa for a carbon content in the original "carbide" of 13.2 mass %. The practically linear behavior of the concentration dependence of the Rockwell hardness, uncorrelated with the bending breaking stress, has been noted in both papers.

The described effect of the carbon content on the properties of chromium carbide–nickel alloys containing 15 mass % Ni is connected with the change in their morphology and phase composition. Thus when using "chromium carbide" containing 12.4 mass % C as the original hard component, according to the Cr–Ni–C phase diagram the sintered alloy contains 18.9 mass % of the phase (Cr_7C_3). For 12.9 mass % carbon in the original "carbide," the amount of the phase based on Cr_7C_3 decreases by almost a factor of four and becomes 5.3 mass %. Further increase in the carbon content in the "carbide" up to 13.3 mass % leads to the appearance of graphite in the alloys, the amount of which increases up to 0.5 mass % for 13.8 mass % C. Thus for a carbon content in the original "carbide" up to 13.1 mass %, the alloy contains a mixture of (Cr_3C_2) and (Cr_7C_3); and if the carbon content is greater than 13.3 mass %, the alloy contains (Cr_3C_2) and graphite. From the above it is clear that it is not advisable to use Cr_3C_2 of stoichiometric composition for preparation of commercial alloys based on this system, because during sintering partial decomposition of this carbide occurs along with dissolution of chromium in the nickel and liberation of free carbon.

Thus, from the data presented it follows that the maximum level of the bending breaking stress (in this case, this indicates the optimal combination of the measured properties) can be displayed by KKhN and KKhNF alloys made from the two-phase region (Cr_3C_2) + (Ni) or the three-phase region (Cr_3C_2) + (Ni) + (Cr_7C_3) near the lower boundary (with respect to carbon) between these phase fields. In order to obtain KKhNF-15 alloys, the carbon content in the original "chromium carbide" should be about 13.2 mass % , i.e., it should be somewhat lower than the stoichiometric Cr_3C_2 (13.34 mass % C).

REFERENCES

23Pir: M. Pirani and H. Alterthum, "A method for melting point determination in high-melting metals," Z. Elektrochem., **29**, No. 1/2, 5-8 (1923).

40Mur: T. Murakami, S. Takeda, K. Mutsuzaki, and T. Murase, "The equilibrium diagram of the Ni–Cr–C system," Nippon Kinzoku Gakkaishi (J. Japan Inst. of Metals), **4**, No. 7, 189-12518 (1940); cited in [95Ter].

51Hes: J. B. Hess, "A modification of the Cohen procedure for computing precision lattice constants from powder data," Acta Cryst., **4**, No. 3, 209-215 (1951).

55Kos: W. Köster and S. Kabermann, "The ternary nickel–chromium–carbon system," Arch. Eisenhüt., **26**, No. 10, 627-630 (1955).

61Gri: V. V. Grigor'eva and V. M. Klimenko, Alloys Based on Chromium Carbide [in Ukrainian], Vid-vo AN URSR, Kiev (1961).

64Lis: V. E. Listovnichii, "Calculation of the emissivity of cylindrical cavities," Inzh.-Fiz. Zh., **7**, No. 11, 32-35 (1964).

69Rud: E. Rudy, Ternary Phase Equilibria in Transition Metal–Boron–Carbon–Silicon Systems. Part V. Compendium of Phase Diagram Data: Tech. Rep. AFML-TR-65-2, U.S. Air Force Materials Laboratory (1969).

71Koch: Yu. A. Kcherzhinskii, E. A. Shishkin, and V. I. Vasilenko, "DTA apparatus with thermocouple sensor up to 2200°," in: Phase Diagrams of Metallic Systems [in Russian], Nauka, Moscow (1971), pp. 245-249.

71Tel: V. S. Telegus and Yu. B. Kuz'ma, Visn. L'viv. Univ., Ser. Khim, **12**, 28-33 (1971).

74Lob: K. Löbl, H. Tüma, and M. Ciznerova, "Activity of carbon in the Ni–Cr–C system in the carbon solubility zone," Mémoires Scientif. Rev. Métalurg., **71**, No. 5, 271-279 (1974).

75Tum: H. Tüma and M. Ciznerova, "Activity of carbon in the Ni–Cr–C system in the region of chromium carbide Cr_7C_3 precipitation," Kovové Materialy, **13**, No. 6, 779-782 (1975).

77Pou: J. J. Poubeau, "Solubility of carbon in chromium and precipitation of carbides in the metal," Doctoral Thesis in Engineering, Univ. Press, Paris (1977).

77Kli: V. N. Klimenko and V. A. Maslyuk, "Chromium carbide–nickel–phosphorus alloys, their properties and application," Poroshk. Met., No. 1-2, 70-79 (1977).

78Kli: V. N. Klimenko, V. A. Maslyuk, and I. D. Radomysel'skii, "Activation of sintering for chromium carbide–nickel alloys" Poroshk. Met., No. 10, 41-44 (1978).

81Ale: V. I. Alekseev, I. V. Degtyarev, and G. A. Levshin, "Phase diagrams of metallic systems," in: Thermodynamic Calculations and Experimental Methods [in Russian], Nauka, Moscow (1981), pp. 91-98 (1981).

82Tum: H. Tüma and M. Ciznerova, "Thermodynamic investigations and the equilibrium diagram of the Ni–Cr–C system in the nickel-enriched region at a temperature of 1000-1200°C," in Kovové Materialy, **20**, No. 4, 426-443 (1982); H. Tüma and M. Ciznerova, "Thermodynamic investigations and the equilibrium diagram of the Ni–Cr–C system in the nickel-rich corner at 1000-1200°C," Metal. Materials, **20**, No. 4, 450-467 (1982).

84Mac: V. A. Maslyuk, "Structure and properties of KKhNF15 alloys made from chromium carbide powders from different production runs," Porosh. Met. No. 12, 38-40 (1984).

85Pou: J. J. Poubeau and J. Bigot, "Determination of the solubility of carbon in chromium by measuring the electrical resistivity at low temperature," Acta Metall., **33**, No. 6, 1137-1141 (1985).

86Nas: P. Nash, "The Cr–Ni (chromium–nickel) system," Bull. Alloy Phase Diagrams, **7**, No. 5, 466-476; 507-508 (1986).

87Ere: V. N. Eremenko, T. Ya. Velikanova, and A. A. Bondar, "Phase diagram of the Cr–Mo–C system. I. Phase equilibria in the region of crystallization of alloys of the partial Mo–Mo_2C–Cr_7C_3–Cr system," Poroshk. Met., No. 5, 70-76 (1987).

89Sin: M. F. Singleton and P. Nash, "The C–Ni (carbon–nickel) system," Bull. Alloy Phase Diagrams, **10**, No. 2, 121-126 (1989).

90Ven: M. Venkatraman and J. P. Neumann, "The C–Cr (carbon–chromium) system," Bull. Alloy Phase Diagrams, **11**, No. 2, 152-159 (1990).

Mas2: T. B. Massalski, P. R. Subramanian, H. Okamoto, and L. Kasprzak, eds., Binary Alloy Phase Diagrams, 2nd edition, ASM International, Materials Park, Ohio (1990); 3 volumes.

91Nas: P. Nash, Phase Diagrams of Binary Nickel Alloys, ASM International, Materials Park, Ohio (1991).

93Bon: A. A. Bondar, V. A. Maslyuk, and A. V. Grytsiv, "Effect of the composition of the original chromium carbide on the structure and properties of chromium carbide–nickel (KKhN) alloys," in: Phase Equilibria, Stability of Phases, and Metastable States in Metallic Systems [in Russian], Inst. Probl. Materialovedeniya im. I. N. Frantsevicha, NAN Ukrainy, Kiev (1993), pp. 148-153.

95Ter: P. Villars, A. Prince, and H. Okamoto, eds., Handbook of Ternary Alloy Phase Diagrams, ASM International: The Materials Information Society, New York (1995); 10 volumes.